Pergamon

Int. J. Heat Mass Transfer. Vol. 38, No. 16, pp. 2959–2967, 1995

0017-9310/95 $9.50+0.00

0017-9310(95)00079-8

Mass transfer characteristics for a rotating cup-like cylinder

WON NYUN KIM and JAE MIN HYUN†

Department of Mechanical Engineering, Korea Advanced Institute of Science and Technology, Yusungku, Taejon, 305-701, South Korea

(*Received* 20 *October* 1994 *and in final form* 19 *January* 1995)

Abstract—A numerical study is made of flow and mass transfer characteristics for a cup-like cylinder, which rotates steadily about its own central longitudinal axis. This study simulates the earlier mass transfer experiment of Sparrow and Chaboki, which provided only the averaged value of Sherwood number. Comprehensive numerical solutions have been obtained for the Navier–Stokes equations over an extended range of Reynolds numbers. Numerically-constructed flow visualizations exhibit the structures of three-component velocity and concentration fields. The patterns of meridional flows, which are directly responsible for convective transport, are analyzed. The distributions of azimuthal flow are illustrated. Plots of the local Sherwood number at the inner surface of the cup are given. Physically plausible descriptions are presented of the local mass transfer characteristics for both cases of a transferring base endwall and a non-transferring base endwall. The numerical results of the cavity-average Sherwood number are consistent with the previous experimental data.

1. INTRODUCTION

Fluid flow and transport processes involving a rotating solid body pose a basic problem in fluid dynamics research. Convective fluid motions are induced by the rotating body, and these fluid flows give rise to enhanced transfer coefficients between the surface of the body and the fluid. Several geometrically-simple body shapes have been considered, and associated augmentation of transport properties has been documented [1–7]. In particular, transport phenomena in the interior region of a cup-like cylindrical vessel, which rotates about its central axis, are of special interest. As illustrated in Fig. 1, owing to the cylinder rotation, there arise complex fluid motions in the cup interior as well as in the surroundings of the cup. Because of these convective activities, transfer coefficients at the inner cylindrical sidewall and at the base endwall disk of the cup are significantly increased. Determination of these transfer coefficients is important in the design and operation of a multitude of rotating fluid machinery, such as a chemical mixer, centrifuge, etc.

Sparrow and Chaboki [8] conducted a pioneering experimental investigation of mass transfer coefficients for a rotating cup, as sketched in Fig. 1. The actual experimental methodology was the naphthalene sublimation technique, which is known to possess higher degrees of accuracy in assessing transport properties. In the experiments, two variants of boundary conditions were implemented. In one case, referred to as type A, the base endwall disk was equipped such

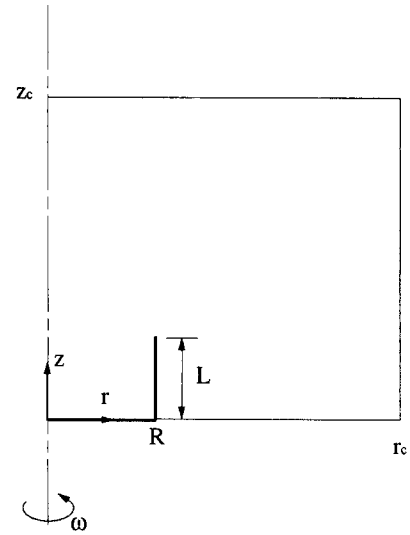

Fig. 1. Problem geometry and computational domain.

that no mass transfer was permitted at that surface. This is equivalent to an adiabatic disk in heat transfer. Mass transfer was allowed only at the cylindrical sidewall surface, at which the naphthalene concentration was kept constant. In the other case, termed type B, both the cylindrical surface and the base disk were maintained at uniform concentration of naphthalene. This is analogous to the constant-temperature wall condition in a heat transfer situation.

Extensive laboratory measurements of Sparrow and Chaboki [8] presented the overall mass transfer coefficients, which were embodied in the average Sherwood number, over ranges of the rotational Reynolds

†Author to whom correspondence should be addressed.

NOMENCLATURE

C	dimensionless concentration	Sh_b	local Sherwood number on the endwall disk
D	diffusivity of concentration	$\overline{Sh_b}$	averaged Sh_b
D	inner diameter of the cylinder, $2R$	Sh_c	local Sherwood number on the cylindrical sidewall
L	height of the cylinder	$\overline{Sh_c}$	averaged Sh_c
R	inner radius of the cylinder	(u, v, w)	velocity components.
(n_c, z_c)	computational domain		
Re	Reynolds number, $\omega R^2/\nu$	*Greek symbols*	
R_o	outer radius of the cylinder		
(r, θ, z)	cylindrical coordinates	ν	kinematic viscosity
Sc	Schmidt number, ν/D	ψ	meridional stream function
Sh	local Sherwood number	ω	angular velocity of the cylinder.
$\overline{Sh}$	total averaged Sherwood number		

number (Re) and of the cylinder aspect ratio (L/D, where L and D denote the height and diameter of the cylinder, respectively). Utilitizing these data, experimental correlations were suggested for high Reynolds numbers, $Re \gtrsim O(10^3)$. These expressed the overall Sherwood number in the form:

$$\overline{Sh} = a\,Re^m (L/D)^n. \tag{1}$$

The empirically-fitted equation (1) was shown to reproduce adequately the measurement data for the afore-stated two types of boundary conditions.

In summary, these laboratory measurements of ref. [8] provided valuable information on the averaged transfer coefficients for a rotating cup-like container. It is noted, however, that the convective flow structure inside the cup was not examined. In the experiments, no flow visualizations were conducted, and measurements were not given for the field of naphthalene concentration. In ref. [8], only the overall coefficient of mass transfer for the entire inner surface of cup was reported, and the local variance of mass transfer was not scrutinized. It is worthy of mention that no other published accounts are found in the literature which address the fundamental issues of transport phenomenon for a rotating vessel such as the one treated by Sparrow and Chaboki [8].

In this paper, it is proposed to seek comprehensive numerical solutions to the governing Navier–Stokes equation. The main advantage of numerical approaches is that details of flow and concentration fields, both at the solid surfaces and in the interior region of the cup, can be described. The global structures of flow and concentration, in the cup interior and in the surroundings close to the cup opening, are essential in ascertaining the impact of rotation-induced convection on the augmentation of transport processes. In the present efforts, numerical solutions are procured in the parameter ranges comparable to the experimental conditions of Sparrow and Chaboki. The numerical results thus obtained are in accord with the measurement data of overall mass transfer coefficients. These endeavors give credence to the present numerical methods; and, based on these validations, numerical computations will be extended to encompass broader ranges of Re and L/D than those of Sparrow and Chaboki. As stressed earlier, descriptions will be rendered of three-component flow and of concentration fields in the rotating cup. Numerically-constructed flow visualizations will be made, and these illustrate the convective characteristics of mass transfer. Systematically-organized computations illuminate the parametric dependence of transfer properties on Re and L/D as well as on the type of boundary conditions imposed on the body surfaces. On balance, the present paper represents an expanded and reinforced numerical model counterpart to the preceding experimental program of Sparrow and Chaboki.

2. FORMULATION AND NUMERICAL MODEL

In reference to the configuration of Fig. 1, the inner radius and height of the cup are respectively R and L, and ω denotes the rotation rate of the cup. The flow is governed by the Navier–Stokes equations of motion. For a cylindrical coordinate frame (r, θ, z), with corresponding velocity components (u, v, w), these equations in dimensionless form are written as

$$u\frac{\partial u}{\partial r} + w\frac{\partial u}{\partial z} - \frac{v^2}{r} = -\frac{\partial p}{\partial r} + \frac{1}{Re}\left(\frac{\partial^2 u}{\partial r^2} + \frac{1}{r}\frac{\partial u}{\partial r} + \frac{\partial^2 u}{\partial z^2} - \frac{u}{r^2}\right) \tag{2}$$

$$u\frac{\partial v}{\partial r} + w\frac{\partial v}{\partial z} + \frac{uv}{r} = \frac{1}{Re}\left(\frac{\partial^2 v}{\partial r^2} + \frac{1}{r}\frac{\partial v}{\partial r} + \frac{\partial^2 v}{\partial z^2} - \frac{v}{r^2}\right) \tag{3}$$

$$u\frac{\partial w}{\partial r} + w\frac{\partial w}{\partial z} = -\frac{\partial p}{\partial z} + \frac{1}{Re}\left(\frac{\partial^2 w}{\partial r^2} + \frac{1}{r}\frac{\partial w}{\partial r} + \frac{\partial^2 w}{\partial z^2}\right) \tag{4}$$

$$\frac{1}{r}\frac{\partial (ru)}{\partial r} + \frac{\partial w}{\partial z} = 0 \tag{5}$$

$$u\frac{\partial C}{\partial r}+w\frac{\partial C}{\partial z}=\frac{1}{Re\,Sc}\left(\frac{\partial^2 C}{\partial r^2}+\frac{1}{r}\frac{\partial C}{\partial r}+\frac{\partial^2 C}{\partial z^2}\right). \quad (6)$$

In the above, C denotes the dimensionless concentration, and other notations are standard. In the nondimensionalization, length is referenced by R, and velocity by ωR. The dimensionless parameters are Re [$\equiv \omega R^2/\nu$], the rotating Reynolds number; Sc [$\equiv \nu/D$], the Schmidt number, in which ν is kinematic viscosity and D diffusivity of concentration. These physical properties are taken to be constant.

In accordance with the problem statement, the fluid far from the cup is at rest and at constant concentration $C = 0$. Due to the cylinder rotation, fluid motions are generated inside and near the cup. The associated boundary conditions are

$$\begin{aligned} &u = w = 0\, v = 1 \quad \text{at}\, r = 1, 0 \leqslant z \leqslant L/R \\ &u = w = 0\, v = r \quad \text{at}\, 0 \leqslant r \leqslant 1\, z = 0. \end{aligned} \quad (7)$$

For the concentration, in line with the experiments of Sparrow and Chaboki, for type A (a non-transferring base):

$$C = 1 \quad \text{at}\, r = 1, 0 \leqslant z \leqslant L/R$$

and

$$\frac{\partial C}{\partial z} = 0 \quad \text{at}\, 0 \leqslant r \leqslant 1\, z = 0 \quad (8a)$$

and for type B (the cylindrical sidewall and the base endwall disk are at constant concentration)

$$C = 1 \begin{cases} \text{at}\, r = 1, 0 \leqslant z \leqslant L/R \\ \text{at}\, 0 \leqslant r \leqslant 1\, z = 0. \end{cases} \quad (8b)$$

In the experiment of ref. [8], the outer surface of the cylindrical sidewall was non-transferring, i.e.

$$u = w = 0 \quad v = R_o \quad \frac{\partial C}{\partial r} = 0 \quad \text{at}\, r = R_o \quad 0 \leqslant z \leqslant L/R \quad (9)$$

where R_o denotes the non-dimensional radius of the outer surface of the solid wall.

The above system of equations is solved by adopting the well-established numerical algorithm SIMPLER [9]. The particulars of the finite-differencing scheme and solution procedures have been widely publicized, and they need not be recapitulated here. As illustrated in Fig. 1, the calculation domain was taken to be sufficiently large to simulate the experimental circumstances. The outer boundary of the computation domain was set at $r_c = 15.0$ and $z_c = 15.0$. A systematic check was made to ascertain the sensitivity of the results to the size of domain. For several sets of pertinent external parameters, as r_c and z_c were varied between 10.0 and 20.0, the corresponding changes in the computed velocity and concentration fields inside the cup were typically less than 1%. The boundary conditions at the outer surface of this domain were specified as

$$\frac{\partial (ru)}{\partial r} = v = w = 0 \quad C = 0 \quad \text{at}\, r = r_c \quad (10)$$

$$u = v = \frac{\partial w}{\partial z} = 0 \quad C = 0 \quad \text{at}\, z = z_c \quad (11a)$$

$$u = v = w = 0 \quad C = 0 \quad \text{at}\, z = 0 \quad R_o \leqslant r \leqslant r_c. \quad (11b)$$

As seen in equation (11b), the outer boundary condition at $z = 0$ simulates the experimental conditions of ref. [8]; in the experiment, the rotating cup was placed on a large stationary table. Again, it is pointed out that the flow field in the interior of the cup is of concern, and these far-outer conditions are shown to have a negligibly small influence on the interior flows.

At the central axis, symmetry requirements are enforced

$$u = v = \frac{\partial w}{\partial r} = 0 \quad \frac{\partial C}{\partial r} = 0 \quad \text{at}\, r = 0. \quad (12)$$

A staggered and stretched mesh was selected, with the grid points clustered near the solid boundaries. Correspondingly fewer grid points were employed at large radii and heights in the computational domain. The actual thickness of the solid cylindrical sidewall of the experiment was not stated in ref. [8]. In the present study, $R_o = 1.01$ was used. It is noted that the conditions at the outer surface of the non-transferring cylindrical wall ($r = R_o$) have minimal impact on the global flow development inside the cup. Therefore, the precise value of R_o is of little concern here. Extensive sensitivity tests were conducted of the computed results to grid spacing and stretching formula. These exercises confirmed satisfactory grid-convergence of the results. For most calculations, a grid network of 60×70 in the (r–z) plane was adopted.

3. RESULTS AND DISCUSSION

In conformity with the naphthalene experiment of ref. [8], $Sc = 2.5$, and $L/R = 1.0$ in the computations. The range of Re encompassed $30 \lesssim Re \lesssim 3500$, although the experiment of ref. [8] covered only the high-Re regime $Re \gtrsim 800$. The objective here is to undertake a comprehensive simulation such that eminent flow characteristics for relatively low Re values may also be identified. In the present mass transfer simulations, the velocity field and concentration field are not coupled. It follows that, for both type A and type B, the flow pattern is the same; only the concentration field differs.

The numerical results are now processed to disclose the three-component velocity structure and concentration. Of particular interest is the meridional flow (u, w) pattern in the (r–z) axial plane. It is convenient to introduce the meridional stream function ψ, which is defined such that

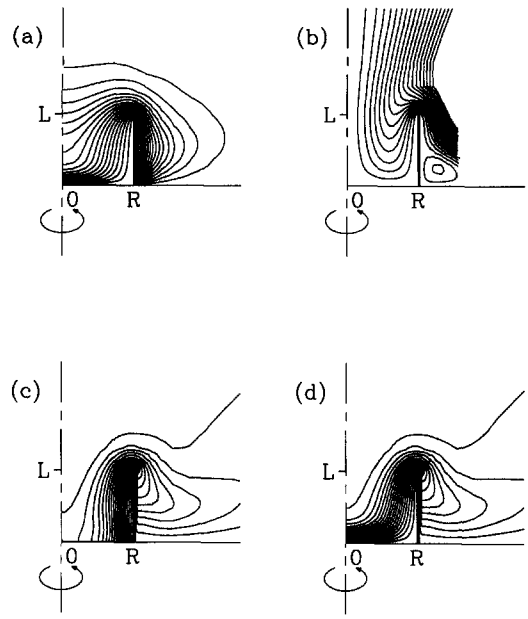

Fig. 2. $Re = 50$. The number of contours is 20. (a) Angular velocity (v/r) field; (b) plots of meridional stream function ψ; (c) concentration (C) field for type A; (d) concentration (C) field for type B.

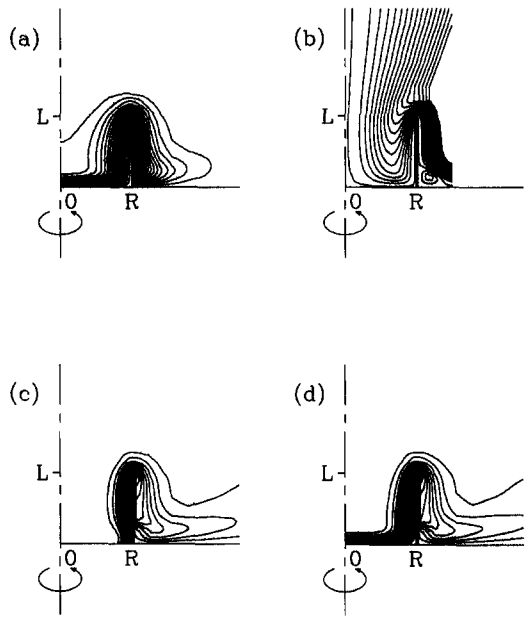

Fig. 3. Same as in Fig. 2, except for $Re = 200$.

$$u = \frac{1}{r}\frac{\partial \psi}{\partial z}$$

$$w = -\frac{1}{r}\frac{\partial \psi}{\partial r}.$$

The behavior of meridional flow is directly responsible for the convective enhancement of transport phenomena [4–7]. In Figs. 2–5, a series of plots, illustrating ψ and C, are given for varying values of Re. First, the

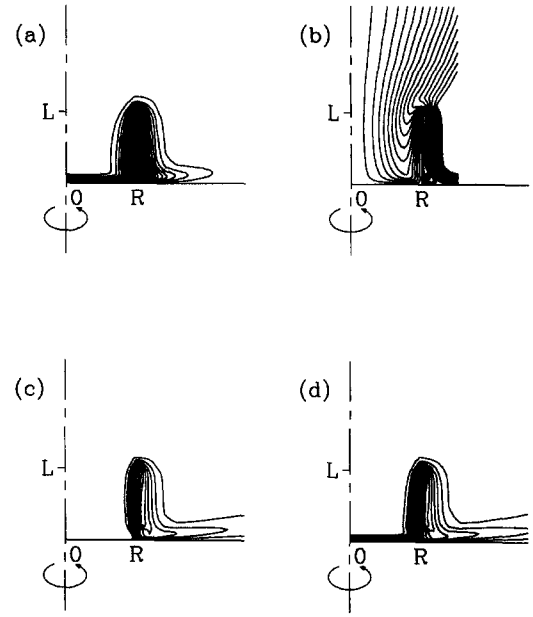

Fig. 4. Same as in Fig. 2, except for $Re = 800$.

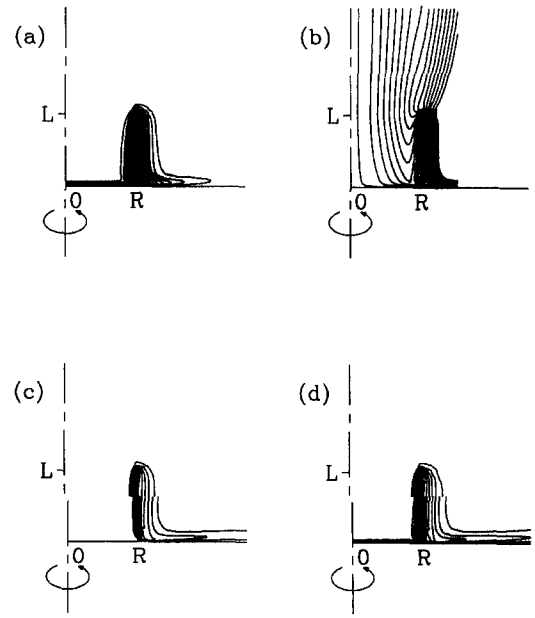

Fig. 5. Same as in Fig. 2, except for $Re = 3200$.

global flow shape is characterized. In general, the rotation of the endwall disk of the cup induces axial flow toward the base from the surroundings. This is a well-documented elementary flow driven by a rotating disk. For high Re, the Ekman boundary layer is formed on the disk and the axial flow is scaled with $Re^{-1/2}R\omega$ (dimensional). This is the consequence of the celebrated Ekman layer pumping effect [10]. In the present problem, since the base of the cup is finite in size and shrouded by the cylindrical wall, the downward axial flow has to move radially outward at moderate and large radii. At large radii near the cylindrical wall

in the interior of the cup, due to the constraint of mass continuity, an upward flow is maintained to exit into the surroundings. The overall circuit of meridional fluid motions may thus be described as a kind of washing process. Namely, fresh fluid is drawn from the surroundings into the cup interior, and while traveling over the surfaces of the base and of the cylindrical wall, the fluid washes off the naphthalene. This naphthalene-enriched fluid leaves through the cup opening at large radii and enters into the surroundings [6, 7].

Figure 2 exemplifies the results for low *Re*. In this case, the convective activity due to the rotation of the cup is comparatively weak, as demonstrated in Fig. 2a. The general flow structure exhibits the above-described qualitative pattern. For low *Re*, the concentration field is heavily influenced by conduction. In Fig. 2c, in the bulk of the cup interior, concentration decreases fairly monotonically from the cylindrical wall toward the axis. Since the base disk is non-transferring, the iso-concentration lines encounter the base perpendicularly. In Fig. 2d, the base is transferring, and concentration decreases almost linearly from the solid surfaces toward the central interior region. Considerable influence of conduction is also discernible in Fig. 2d.

At large *Re*, it is conspicuous that the boundary-layer-like flow character is manifested. The penetration of the fluid into the cup interior is more effective, as seen in Fig. 5b. The boundary layers, both on the disk and the cylindrical wall, are distinct and thin. Figures 5c and d indicate that, at large *Re*, naphthalene tends to be confined to thin boundary layers adjacent to the solid walls, and in the bulk of the interior core of the cup concentration is very weak. A gradual shiftover of the flow character, from one with a substantial effect of conduction (Fig. 2) to one with an overwhelming influence of convection (Fig. 5), is depicted in Figs. 2–5. It is interesting to point out the qualitative difference in the C-field between type A and type B at large *Re*, as illustrated in Figs. 5c and d. When the base is non-transferring, the fluid that reaches the vicinity of the bottom of the cylindrical wall has very low concentration. Therefore, the concentration boundary layer on the cylindrical wall is thin and distinct. In the case of a transferring base, a concentration boundary layer is present on the disk. As a result, the fluid that moves upward in the boundary layer on the cylindrical wall has already been enriched by the base disk. Consequently, the concentration boundary layer on the cylindrical wall is thicker and comparatively less distinct than for the case of a non-transferring disk. The flow visualizations and the depiction of the C-fields are consistent with the afore-stated physical portrayals.

The numerical results are analyzed further to permit a quantitative evaluation of the effect of *Re*. Figure 6 illustrates the radial profiles of axial velocity. At the mid-height of the cup interior (Fig. 6a for $z = 0.5L/R$), as *Re* increases, the intensification of w, as well as the thinning of the boundary layer at the cylindrical wall, is evident. At the opening of the cup (Fig. 6b for $z = 1.0L/R$), a similar trend is visible. However, at this height, the magnitude of the upward motion is greater and the boundary layer is thinner than in the interior regions (note the difference in the scales of the ordinates of Fig. 6a and 6b).

Representative vertical profiles of the radial velocity at several radial positions are displayed in Fig. 7. In the central interior region, curves for $r = 0.3$ and $r = 0.5$ demonstrate that the cylindrical sidewall effects are insignificant. At large radii (see the curve for $r = 0.8$), considerable sidewall effects are discernible. At low values of *Re*, the horizontal velocities in the central region are directed radially outward in a broad area in the bottom portion of the cavity, and u decreases monotonically with height. As *Re* increases, it is evident that the boundary layer-type flow character prevails. As shown in Fig. 7d, at large *Re*, in the bulk of the interior, u is practically zero. Only in the thin and distinctive Ekman layer on the base disk is a paradigmatic variation of u with height seen. The effect of the sidewall on the flow behavior is comparatively small when *Re* takes a large value.

The structure of the azimuthal velocity v is now examined. Figure 8 depicts vertical profiles of the angular velocity (v/r). Note that, due to the rotation of the cup, the primary flow of $O(1)$ exists in the azimuthal direction. When *Re* is low (see Fig. 8a), the entire flow field is heavily influenced by viscosity effects. The velocity variations appear to be fairly monotonic in much of the interior. As *Re* increases, the establishment of boundary layer is evident, and the effect of the no-slip condition at the cylindrical wall is confined to a narrow strip close to the wall. At large *Re*, as seen in Fig. 8d, the bulk of the interior core is nearly non-rotating. The rotating fluids are concentrated to the Ekman layer on the disk and to the cylindrical wall boundary layer. This is in confirmation of the much-studied behavior of bounded rotating fluid motions at large *Re* [10–12].

Now, compiling the numerical data, the local Sherwood number *Sh*, $Sh \equiv \partial C/\partial n$, where n is the coordinate normal to the solid wall surface, has been calculated in Fig. 9. Figure 9a demonstrates the *Sh*-distribution on the cylindrical wall for type A. For this case, the base is non-transferring ($Sh_b \equiv 0$ at the base); therefore, the fluid that reaches the bottom region of the cylindrical wall is of very low concentration, since the fluid has not been enriched with naphthalene while traveling over the disk. Because of a large concentration difference between the fluid and the cylindrical wall, mass transfer is vigorous and the resulting Sh_c is high in the bottom portion of the cylindrical wall. As the fluid flows upward along the cylinder wall around intermediate heights, the fluid becomes enriched in naphthalene. This reduces the difference in naphthalene concentration between the fluid and the solid wall; consequently, Sh_c decreases in these regions. Near the opening of the cup, as dis-

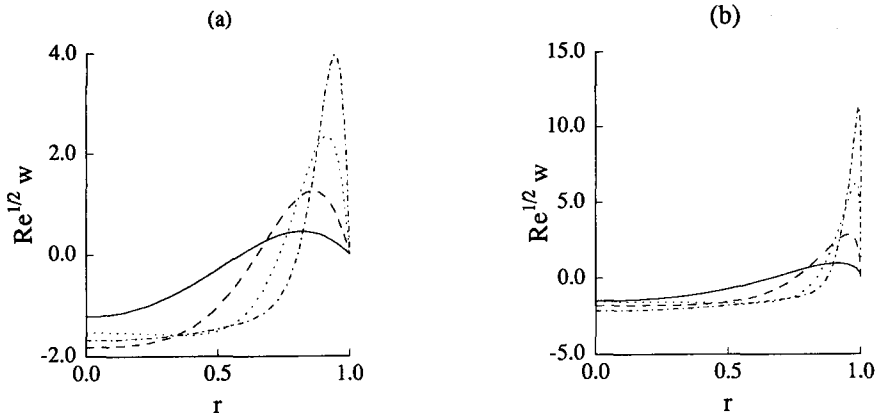

Fig. 6. Radial profiles of axial velocity w. (a) $z(R/L) = 0.5$, (b) $z(R/L) = 1.0$. (——) $Re = 50$; (— —) $Re = 200$; (· · ·) $Re = 800$; (— · —) $Re = 3200$.

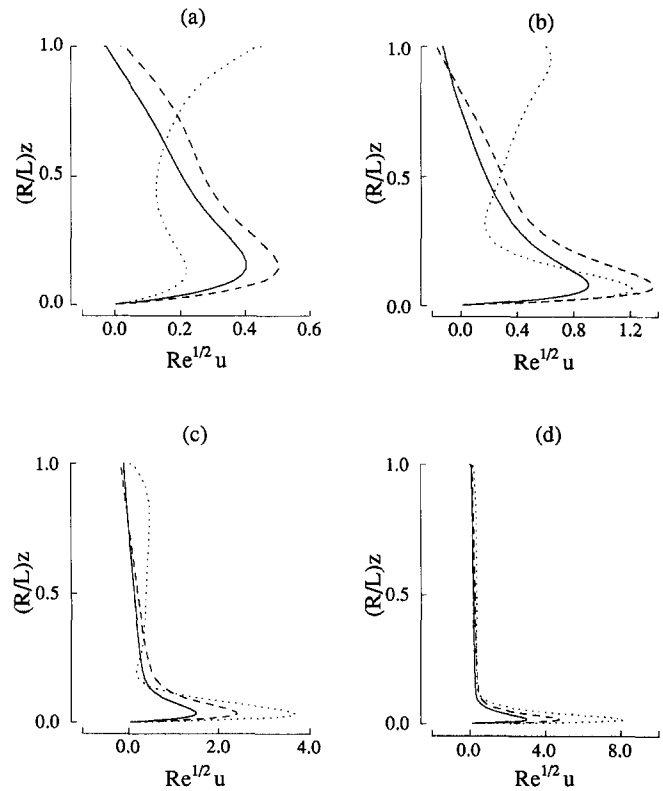

Fig. 7. Axial profiles of radial velocity u. (a) $Re = 50$; (b) $Re = 200$; (c) $Re = 800$; (d) $Re = 3200$. (——) $r = 0.3$; (— — —) $r = 0.5$; (· · ·) $r = 0.8$.

played in Figs. 2–5, the fluid makes a sharp turn radially outward to exit into the surroundings. This generates steep velocity gradients, together with the thinning of the concentration boundary layer, in this localized zone. Therefore, Sh becomes large locally, and the Sh-behavior in Fig. 9a is compatible with this physical reasoning. The Sh-distributions for type B, for which both the base and the cylindrical wall are transferring, are displayed in Fig. 9b and c. As portrayed in the flow visualization pictures of Figs. 2–5, fresh fluid is sucked into the cavity interior over much of small and moderate radii. This fluid, with almost zero concentration, penetrates down to the base disk over this radial extent. Consequently, mass transfer from the base ($C = 1.0$) to the fluid is vigorous, which turns up in a large and radially-uniform value of Sh_b over much of the disk (see Fig. 9b). When the fluid reaches large radii close to the corner adjoining the bottom of the cylindrical wall, the fluid has been appreciably enriched with naphthalene. This brings forth a drop in mass transfer rates, which shows up in decreasing Sh at large radii of the disk as well as in the lower zones of the cylindrical wall. At mid-heights of the cylindrical wall, because of intensified con-

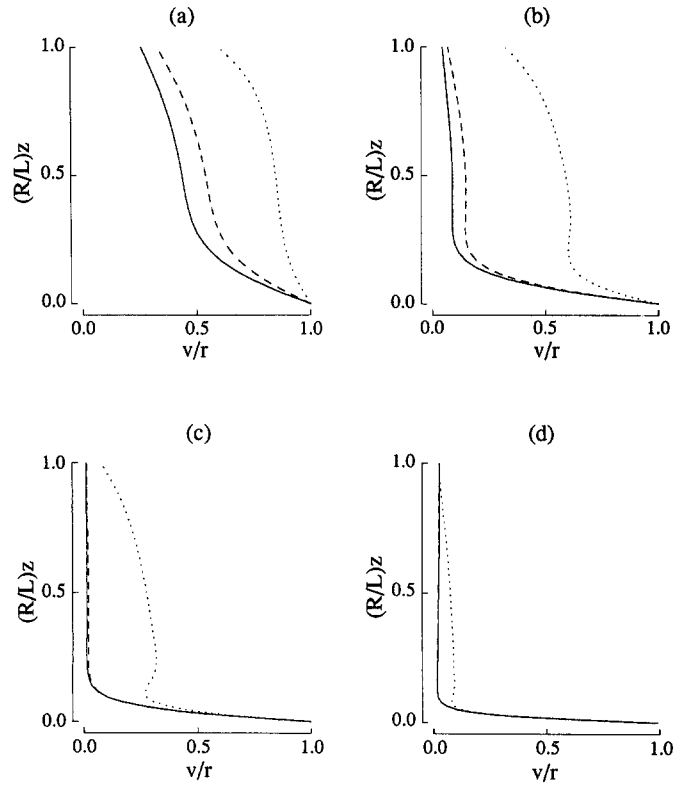

Fig. 8. Angular velocity (v/r) structures. (a) $Re = 50$; (b) $Re = 200$; (c) $Re = 800$; (d) $Re = 3200$. (——) $r = 0.3$; (– – –) $r = 0.5$; (· · ·) $r = 0.8$.

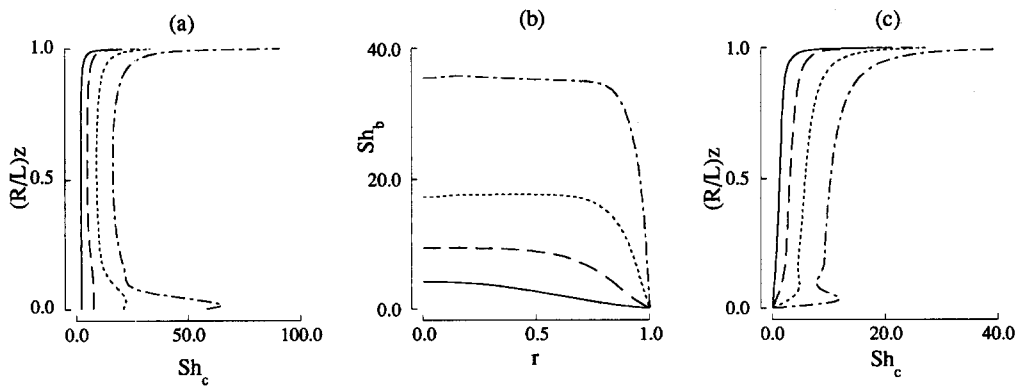

Fig. 9. Distributions of the local Sherwood number. (a) Local Sherwood number Sh_c at the cylindrical wall, type A; (b) local Sherwood number Sh_b at the base disk, type B; (c) local Sherwood number Sh_c at the cylindrical wall, type B. (—) $Re = 50$; (– – –) $Re = 200$; (· · ·) $Re = 800$; (— · —) $Re = 3200$.

vective flows in the vertical boundary layer at the cylindrical wall, Sh_c tends to increase slightly with height. Near the opening of the cup, due to a sharp turn of the flow direction, as the fluid exits into the surroundings, the thickness of concentration boundary layer decreases. This, together with large velocity gradients, gives rise to substantially enhanced transfer processes. Large values of Sh_c in the opening region of the cylindrical wall of the cup, as demonstrated in Fig. 9c, are indicative of the reasonableness of the above physical interpretations. Note that the average value of Sh_c for type A is generally larger than for type B (note the difference in scales for Sh_c between Fig. 9a and c). This observation is in accord with the earlier findings of ref. [8].

Finally, the computed data for local Sh are integrated to produce the mean value $\overline{Sh}$, which was previously reported by the experiment in ref. [8]. Figure 10 illustrates cross-comparisons between the measured value of $\overline{Sh}$ and the present numerical results. It should be mentioned that the experimental data of ref. [8] were secured only for the large-Re regime, i.e. $Re \gtrsim 800$. For both type A and type B, it is evident that two sets of data are in close agreement. The

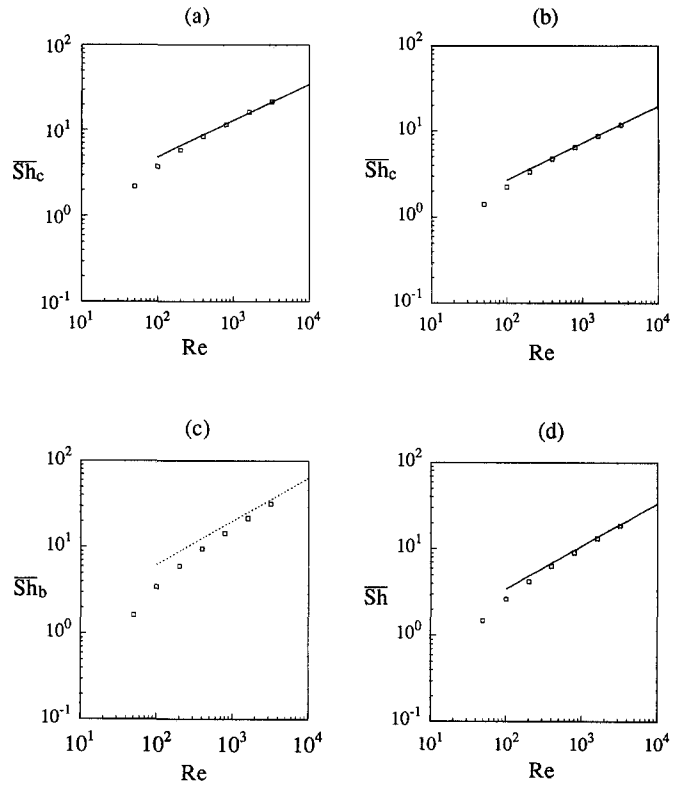

Fig. 10. Averaged Sherwood number $\overline{Sh}$ vs Re. (a) $\overline{Sh}_c$ at the cylindrical wall, type A; (b) $\overline{Sh}_c$ at the cylindrical wall, type B; (c) $\overline{Sh}_b$ at the base disk, type B; (d) $\overline{Sh}$ at the entire wall surface, type B. (——) Experimental results of ref. [8]; (□) the present numerical data; (· · ·) result for rotating disk of ref. [1, 8].

present results are in support of the empirically-fitted correlation of ref. [8]:

$$\overline{Sh} = 0.283 Re^{0.485}(L/(2R))^{-0.465}$$

which is plotted as the solid line in Fig. 10. It is remarked that, as anticipated, the overall mass transfer coefficient $\overline{Sh}$ is larger for the case of a non-transferring base. This finding was stated in ref. [8], and the present numerical results are consistent with the experimental observations.

4. CONCLUSION

Fluid inducement into the cup interior intensifies as Re increases. At large Re, the global flow pattern is convectively controlled, with distinct and thin boundary layers present on the solid walls. The concentration boundary layer at the cylindrical wall is thicker for the case of a transferring base (type B) than for a non-transferring base (type A). At small and intermediate radii, w is negative and fairly uniform in the radial direction. At large radii near the cylindrical wall, large positive values of w are seen.

At large Re, the angular velocity (v/r) is very small in much of the cup interior. Only in the regions adjacent to the solid walls, v/r is appreciable.

Detailed descriptions of the local Sherwood number are given. On the cylindrical wall, Sh becomes large near the opening of the cup. In the case of a transferring base, Sh is fairly uniform at small and moderate radii of the disk, and Sh decreases radially at large radii close to the cylindrical wall.

The computed mean Sherwood number $\overline{Sh}$ is in close agreement with the available experimental data of ref. [8]. The overall value of $\overline{Sh}$ is larger for a non-transferring base than for a transferring base.

Acknowledgment—This work was supported in part by research contracts from Tong Yang Magic Co. and from Tong Yang Industrial Machinery Co. of Korea.

REFERENCES

1. E. M. Sparrow and J. L. Gregg, Heat transfer from a rotating disk to fluids of any Prandtl number, *ASME J. Heat Transfer* **81**, 249–251 (1959).
2. F. Kreith, Convection heat transfer in rotating systems, *Adv. Heat Transfer* **5**, 129–251 (1968).
3. S. M. Tieng and A. C. Yan, Experimental investigation on convective heat transfer of heated spinning sphere, *Int. J. Heat Mass Transfer* **36**, 599–610 (1993).
4. S. Gilham, P. C. Ivey, J. M. Owen and J. R. Pincombe, Self-induced flow in a rotating tube, *J. Fluid Mech.* **230**, 505–524 (1991).
5. S. Gilham, P. C. Ivey and J. M. Owen, Self-induced flow and heat transfer in a rotating tube, *Int. J. Heat Fluid Flow* **14**, 27–36 (1993).

6. R. Shimada, S. Naito, S. Kumagai and T. Takeyama, Enhancement heat transfer from a rotating disc using a turbulence prometer (in Japanese), *Trans. JSME (B)* **53–487,** 984–990 (1988).
7. K. Hirose, T. Yokoyama and M. Ouchi, Heat convection on brake disk (in Japanese), *31st Heat Transfer Symp. Japan*, Sapporo, Paper number E245 (1994).
8. E. M. Sparrow and A. Chaboki, Heat transfer coefficients for a cup-like cavity rotating about its own axis, *Int. J. Heat Mass Transfer* **25,** 1333–1341 (1982).
9. S. V. Patankar, *Numerical Heat Transfer and Fluid Flow*. Hemisphere/McGraw-Hill, New York (1980).
10. H P. Greenspan, *The Theory of Rotating Fluid*. Cambridge University Press, Cambridge (1968).
11. J. M. Hyun, Flow in an open tank with a free surface driven by the spinning bottom, *ASME J. Fluids Engng* **107,** 495–499 (1985).
12. T. G. Lim, S. Choi and J. M. Hyun, Transient interface shape of a two-layer in an abruptly rotating cylinder, *ASME J. Fluids Engng* **115,** 324–329 (1993).